Polymer 206 (2020) 122849

Contents lists available at ScienceDirect

Polymer

journal homepage: http://www.elsevier.com/locate/polymer

Microphase-separated structures of ion gels consisting of ABA-type block copolymers and an ionic liquid: A key to escape from the trade-off between mechanical and transport properties

Haruna Mizuno [a], Kei Hashimoto [a,b], Ryota Tamate [a,c], Hisashi Kokubo [a], Kazuhide Ueno [a], Xiang Li [d], Masayoshi Watanabe [a,b,*]

[a] Department of Chemistry and Life Science, Yokohama National University, 79-5 Tokiwadai, Hodogaya-ku, Yokohama, 240-8501, Japan
[b] Institute of Advanced Sciences, Yokohama National University, 79-5 Tokiwadai, Hodogaya-ku, Yokohama, 240-8501, Japan
[c] Center for Green Research on Energy and Environmental Materials, National Institute for Materials Science, 1-1, Namiki, Tsukuba, Ibaraki, 305-0044, Japan
[d] Institute for Solid State Physics, The University of Tokyo, 5-1-5 Kashiwanoha, Kashiwa, Chiba, 277-8581, Japan

ARTICLE INFO

Keywords:
Ionic liquid
Block copolymer
Microphase separation
Ionic conductivity
Mechanical property
ORCID

ABSTRACT

Upon combination of an ionic liquid (IL) with an amphiphilic ABA-type triblock copolymer, the insoluble A blocks aggregate to form mechanical frameworks and the soluble B blocks form ion-transport paths by incorporating the IL. Consequently, a self-standing ion gel, exhibiting the characteristic high ionic conductivity of ILs, can be obtained. In this study, we investigated the effect of microstructures formed by the block copolymer (spherical, cylindrical, gyroid, and lamellar structures) on the ionic conductivity and mechanical properties of the ion gel by focusing on the microstructures. As a result, an ion gel that formed an isotropic bicontinuous structure was successfully obtained via a heat-induced order-order transition. The structure was maintained even at room temperature, and the ion gel having a bicontinuous structure exhibited favorable mechanical properties (storage modulus, $G' \sim 1.0$ MPa) and good ionic conductivity ($\sigma \sim 0.1$ mS cm^{-1}). In contrast, the ion gels having anisotropic structures (cylindrical structure) exhibited weaker mechanical properties and lower ionic conductivity. The characteristics of bicontinuous structures may be the key to resolving the trade-off between mechanical and transport properties of electrolyte materials for electrochemical devices.

1. Introduction

Ionic liquids (ILs) are salts composed entirely of cations and anions that typically have weak Lewis acidity and basicity, respectively, and melt at temperatures lower than 100 °C. They have notable characteristics such as low flammability, low volatility, good thermal and chemical stability, and high ionic conductivity, which are entirely different from those of conventional water and organic solvents [1]. These properties can be controlled by selecting a suitable combination of a cation and an anion that can bestow properties such as high affinity toward gas [2], biopolymers [3], and synthetic polymers [4] on ILs. Therefore, ILs are sometimes called a 'third solvent' or a 'designer solvent'. The high affinity to polymers enables us to make composite materials comprising ILs and polymer networks, namely, ion gels [4b,5]. Ion gels have attracted attention as ion-conductive materials with semi-solid and self-standing characteristics, especially for electrochemical devices. The most notable characteristics of ion gels are softness and ion-transport property. Thus, a polymer actuator using ion gels can reproduce a soft motion similar to the movement of living things, which can be used to develop artificial muscles of robots [6]. The application area of ion gels is wide-ranging; they may be used as a gas separation membrane [2c,7], semi-solid electrolyte for capacitors [8], batteries [9], fuel cells [10], and solar cells [11]. In these applications, the trade-off between mechanical strength and ionic conductivity (or ion-transport property) is a critical issue. For a durable and robust ion gel, the content of the polymer network should be high, while a low content of the IL results in low ionic conductivity. To resolve this trade-off, various chemically cross-linked polymer networks in IL, such as polymerization-induced continuous network [12], homogeneous polymer network [13], composite of polymer network and inorganic particles [14], and double-network [15] have been proposed.

Gelation based on the microphase separation phenomenon of block

* Corresponding author. Department of Chemistry and Life Science, Yokohama National University, 79-5 Tokiwadai, Hodogaya-ku, Yokohama 240-8501, Japan.
E-mail address: mwatanab@ynu.ac.jp (M. Watanabe).

https://doi.org/10.1016/j.polymer.2020.122849
Received 14 April 2020; Received in revised form 25 June 2020; Accepted 23 July 2020
Available online 7 August 2020

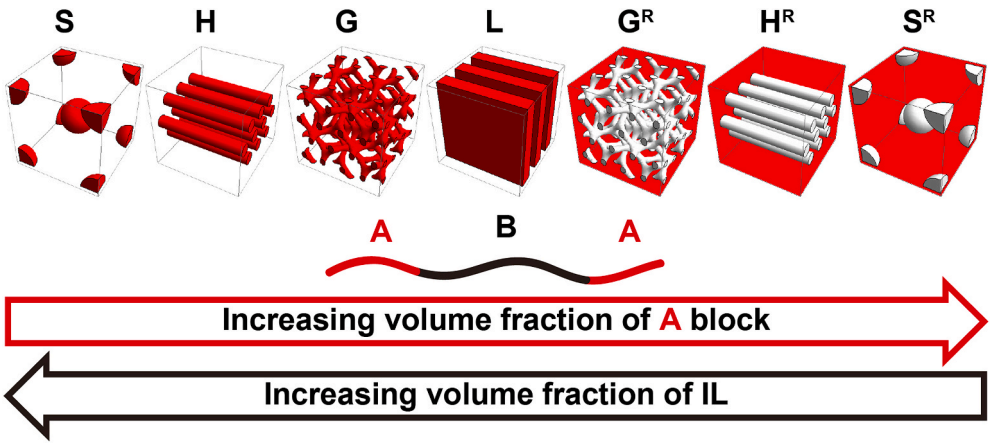

Fig. 1. Typical microphase-separated structures formed by AB-type block copolymers. S: spheres; H: hexagonally-packed cylinders; G: gyroids; L: lamellas; G^R: reverse G; H^R: reverse H, S^R: reverse S.

copolymers composed of blocks having different compatibilities with ILs is one of the simplest and highly versatile gelation methods for ILs. The thermoplastic characteristics of physical cross-linking points bestow good formability on ion gels, which is different from the chemical ion gels mentioned above. During the gelation of ABA-type triblock copolymers consisting of insoluble A blocks and a soluble B block, the insoluble A blocks aggregate to form mechanical flameworks while the soluble B segments make ion-transport paths by incorporating ILs [16]. Observation of nm-order structure of ion gels using transmission electron microscope (TEM), atomic force microscope (AFM), and small angle X-ray scattering (SAXS) shows that block copolymers in ILs form ordered structures analogous to diblock copolymer melts such as spheres (S), hexagonally-packed cylinders (H), their reverse structures (S^R and H^R), lamellas (L), and bicontinuous structures such as gyroids (G and G^R), depending on the volume fraction of the A block (f_A) and IL content (Fig. 1) [17]. It has been reported that the microphase-separated structure dramatically affects the mechanical and transport properties of polymer materials,[18] which can be a key to solve the trade-off.

We have previously investigated the correlation between microphase-separated structures and electrolyte properties, including mechanical and ion-transport properties, of ion gels composed of polystyrene-*b*-poly(methyl methacrylate)-*b*-polystyrene (PSt-*b*-PMMA-*b*-PSt, SMS) and a typical IL, 1-ethyl-3-methylimidazolium bis(trifluoromethanesulfonyl)amide ([C_2mim][NTf_2]) [16a,17b]. Regarding the mechanical properties, it was found that the continuity of PSt aggregates significantly contributed to the elastic modulus. On the other hand, the continuity of the ion-conductive path substantially contributed to the ion conductivity. The non-ion conductive PSt aggregates partially interrupted or detoured the ion conduction path, resulting in lowering the ionic conductivity of ion gels. We evaluated the reduction in ionic conductivity depending on the microphase-separated structure using "tortuosity," which is a metric of the complexity of the ion conduction path. The tortuosity of the ion gel depends considerably on the microphase-separated structures. Ion gels with the H or L structure exhibit higher tortuosity than those with the S structure (Fig. 1). In bulk ion gels, the anisotropic H and L structures exhibit a polydomain structure, i.e., grains composed of ordered cylinders or lamellas are randomly packed. In a polydomain structure, the H or L structures aligned vertically and horizontally to the conduction direction are mixed, resulting in a significantly high tortuosity. On the other hand, isotropic structures such as the S structure do not exhibit a polydomain structure, resulting in a good ion conduction path with an ideal tortuosity close to unity.

In this study, we focused on the isotropic gyroid (G) bicontinuous structure. The isotropic G structure is expected to exhibit small tortuosity because of the lack of a polydomain structure, which can result in high ionic conductivity. In terms of mechanical properties, it is expected to exhibit high mechanical strength as well because insoluble PSt segments in the G structure are continuous in the three-dimensions. Therefore, an ion gel having a G structure would have favorable mechanical strength and ionic conductivity, which may resolve the trade-off. There are some reports on the high mechanical and transport properties in diblock copolymers incorporated with salts or polyelectrolytes [19]. However, the compositional range where the block copolymer stably forms a G structure is narrow. In the ion gels system, IL acts as a plasticizing solvent for one of the block copolymer segments, and thus, the phase behavior is different from the previously reported block copolymer systems, resulting in the difficulty in the prediction of the microstructure. To the best of our knowledge, in the ion gel system, there has been no report of the visualization of the G structure being formed by self-assembly in ILs.

In the diblock copolymer melt system, several researchers have reported that increasing the temperature can induce an order-order transition (OOT) from H or L to G structure [20]. Such structural transition increases the elastic modulus, which is correlated with the formation of the continuous phase with cubic symmetry [21]. At high temperatures, the G structure is energetically more stable than the ordered L or H structures. Hillmyer et al. [22] have reported that PSt-*b*-poly(ethylene oxide) (PEO) exhibits OOT at ~200 °C, and successive quenching results in the formation of a stable G structure at room temperature. Based on these results, it was speculated that the same phenomenon could be realized in the ion gel system. Therefore, we prepared the ABA-type block copolymer-based ion gels having a G structure via heating-induced OOT transition. We employed PSt and PEO as terminal and middle blocks, respectively, according to the previous report [22], and aimed to improve the ionic conductivity using PEO with a low glass transition temperature (T_g = −66 °C). To obtain a material with excellent mechanical strength and ionic conductivity, we investigated the ideal composition of the ion gel for forming the G structure by AFM and correlated the mechanical properties and ionic conductivity with the microphase-separated structures.

2. Experimental

2.1. Materials

Prior to its use, PEO (M_n = 4.6 and 10 kDa, Aldrich (USA)) was dissolved in toluene and dried under reduced pressure at 50 °C to remove water. A chain transfer agent (CTA), 2-(dodecylthiocarbonothioylthio)-2-methylpropionic acid, was purchased from Aldrich (USA) and used without further purification. Styrene was purchased from Tokyo Chemical Industry (Japan) and the polymerization

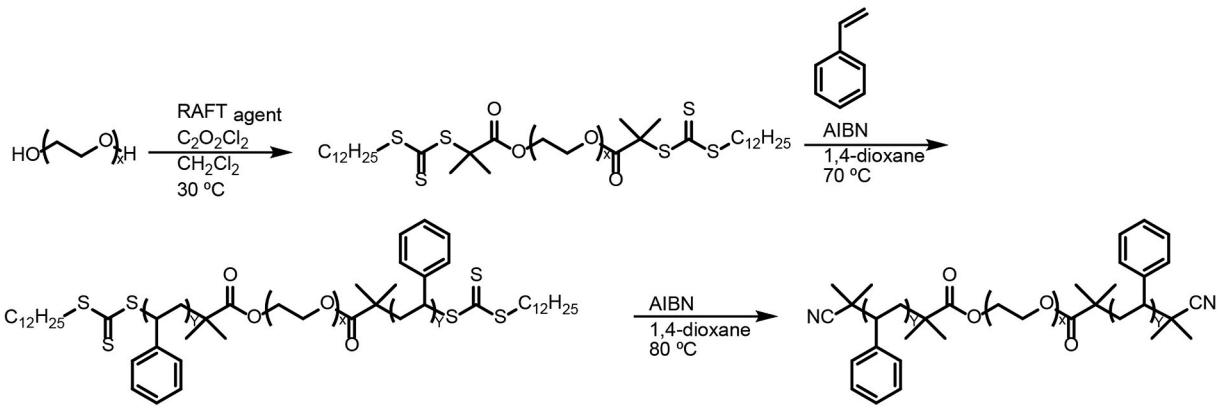

Scheme 1. Synthetic procedure for PSt-*b*-PEO-*b*-PSt.

inhibitor was removed by column chromatography using alumina powder. A radical initiator, 2,2′-azobis(isobutyronitrile) (AIBN) was purchased from Wako Chemical (Japan) and purified by repetitive recrystallization using methanol as a solvent. Dichloromethane, toluene, tetrahydrofuran (THF), hexane, and 1,4-dioxane (super dehydrated) were purchased from Wako Chemical (Japan). Oxalyl chloride was purchased from Tokyo Chemical Industry (Japan). These reagents were used without further purification.

2.2. Synthesis

The IL, [C_2mim][NTf_2], was synthesized and dried before use according to a previous report.[23] The ABA-type triblock copolymer, PSt-*b*-PEO-*b*-PSt (SOS), was synthesized by reversible addition-fragmentation chain transfer (RAFT) polymerization (Scheme 1).

2.2.1. Synthesis of PEO-CTA bifunctional macroinitiator

CTA (4.09 g, 11.2 mmol) and oxalyl chloride (1.4 mL, 18.3 mmol) were dissolved in dichloromethane (60 mL) in an Ar-filled flask, and the solution was stirred at 30 °C for 2 h. Subsequently, CO_2 gas and solvent were removed from the mixture under reduced pressure, and a solution of PEO (M_n = 10 kDa, 11.2 g, 1.12 mmol) in dichloromethane (36 mL) was added to the residue. The solution was stirred at 30 °C for 18 h. The reaction solution was precipitated into an excess amount of hexane, and the resulting polymer was collected by filtration. The polymer was purified by repetitive precipitation using THF (good solvent) and hexane (poor solvent) and dried under vacuum at 40 °C overnight. The purified PEO-CTA macroinitiator was obtained as a pale-yellow powder. PEO-CTA having smaller M_n (4.6 kDa, 3.47 g, 0.753 mmol) was also synthesized using the same method.

2.2.2. Synthesis of ABA-type triblock copolymer

The synthesized PEO-CTA macroinitiator (M_n = 10 kDa, 1.00 g, 0.0934 mmol) was dissolved in styrene (4.6 mL, 40.0 mmol) in an Ar-filled flask. Ar was bubbled through the solution at 25 °C for 30 min to remove dissolved oxygen. Then, AIBN/1,4-dioxane solution (10 mg/20 mL), from which dissolved oxygen had already been removed by Ar bubbling, was poured into the flask. The polymerization reaction was conducted at 100 °C for 15 h with stirring. Successively, the reaction was quenched using liquid nitrogen and exposed to air. The polymer was then purified by precipitation into an excess amount of hexane and collected by filtration. The polymer was purified by repetitive precipitation using dichloromethane (good solvent) and hexane (poor solvent) and dried under vacuum at 40 °C overnight. The purified CTA-PSt-*b*-PEO-*b*-PSt-CTA (conversion: St 34.2%, gas chromatography) was obtained as a pale-yellow powder. CTA was removed by its reaction with excess AIBN in 1,4-dioxane at 80 °C for 1 day. Then, the polymer was purified by precipitation again and dried under vacuum at 40 °C overnight. The purified PSt-*b*-PEO-*b*-PSt was obtained as a white powder. Fig. S1 shows the ^{1}H NMR spectra of the polymers synthesized from PEO (M_n = 10 kDa). The ratio of CTA-modification was calculated from the signals of protons within the PEO main chain and methyl group of CTA (Fig. S1(a), signal (a) and (g), respectively) to be 96%. The volume fraction of PSt (f_{PSt}) was calculated from the signals of protons within the PEO main chain and aromatic ring of PSt (Fig. S1(b), signal (i) and (f), respectively) to be 66.1%. Therefore, we named this polymer SOS-66 in this study. The ^{1}H NMR spectrum obtained after the removal of CTA (Fig. S1(c)) exhibited no signal of CTA, indicating its complete removal.

Table 1
Number average molecular weight (M_n), polydispersity index (PDI), and f_{PSt} of SOS-66 and SOS-84.

Polymer	*M_n (PSt-b-PEO-b-PSt)/kDa* [a]	*PDI* [b]	*f_{PSt} (%)* [c]
SOS-66	8.0-10.0-8.0	1.34	66.1
SOS-84	9.8–4.6-9.8	1.43	83.9

[a] Calculated from the conversion.
[b] Calculated from the gel permeation chromatography (GPC) curves.
[c] Calculated from the density of PSt and PEO.

SOS-84 (f_{PSt} = 83.9%) was also synthesized using a shorter PEO-CTA macroinitiator (M_n = 4.6 kDa). PEO-CTA (1.06 g, 0.200 mmol), styrene (14.1 mL, 123 mmol), and AIBN/1,4-dioxane (20 mg/40 mL) were reacted after degassing at 100 °C for 9 h (conversion of St: 30.6%, GC), followed by the removal of CTA and repetitive precipitation. This SOS was denoted as SOS-84. Fig. S2 shows the gel permeation chromatography (GPC) curves of SOS-66 and SOS-84. The synthesized polymer exhibited monomodal peaks. However, the distribution was broad. To control the molecular weight of PSt blocks, we checked the progress of the reaction several times by gas chromatography. During the check, a little amount of oxygen could enter the reaction vessel, resulting in a partial termination of the reaction. This can be a reason for the wide distribution. However, from the ^{1}H NMR spectra (Fig. S1(b)), we concluded that the reaction was proceeded and the block copolymer was obtained. The M_n, polydispersity index (PDI), and f_{PSt} of the polymers are summarized in Table 1.

2.2.3. Preparation of SOS/[C_2mim][NTf_2] ion gel

The solution of [C_2mim][NTf_2] and SOS in THF (cosolvent) was cast into a mold. THF was gradually evaporated to form an ion gel. The obtained gel was annealed at 180 °C for 1 day to obtain a well-equilibrated microphase-separated structure. The weight fraction of polymer and volume fraction of the soft segment (φ_{soft}, i.e., the sum of the volume fraction of PEO block and IL) were calculated from the feed amount of polymer and IL, and assigned microphase-separated structures are listed in Table S1.

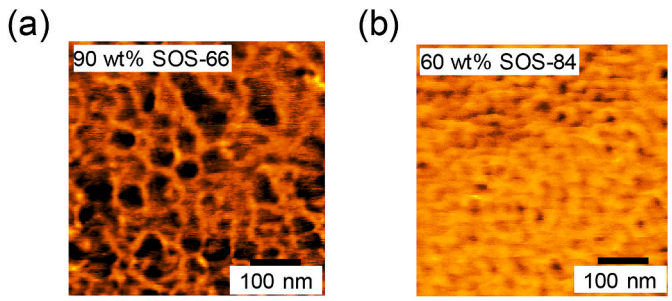

Fig. 2. AFM phase images of (a) 90 wt% SOS-66/[C_2mim][NTf_2] and (b) 60 wt % SOS-84/[C_2mim][NTf_2] ion gels.

2.3. Measurements

2.3.1. Rheological measurement

Rheological measurements were performed on as-prepared disk-shaped ion gels before annealing (thickness: 0.5 mm) using a Physica MCR102 (Anton Paar, Austria) rheometer. A temperature controlling hood (H-PTD200) was attached to MCR102 to stabilize the temperature. A parallel plate (diameter: 12.5 mm) was employed. The frequency (f) and strain (γ) were 1 Hz and 3%, respectively. The sample was gradually heated at a rate of 1 °C min^{-1} and then cooled at the same rate. The temperature dependencies of storage and loss moduli (G' and G'', respectively) were recorded in the first heating and cooling steps.

2.4. Ionic conductivity

The ionic conductivity of the ion gel was estimated from the complex impedance measurements conducted over a frequency range from 5 Hz to 13 MHz (amplitude: 10 mV) using a Hewlett-Packard 4192A LF impedance analyzer. The ion gels were molded into a disk shape (diameter: 1.2 cm; thickness: 0.5 mm) via hot pressing at 150 °C and sealed between two stainless steel electrodes. The measurements were conducted at every 10 °C step from 100 °C to 30 °C (data at 25 °C was also recorded) in the cooling step. Before every impedance measurement, the temperature was equilibrated for at least 1 h to stabilize the sample temperature.

2.5. SAXS analysis

SAXS measurements were conducted on BL-10C (Photon Factory, Japan) with a monochromated X-ray beam (wavelength, $\lambda = 1.00$ Å) using a detector (PILATUS3 2 M, Dectris) at a sample-to-detector distance of 3.1 m. X-rays were directly irradiated onto the sample. The measurements were performed at room temperature for an exposure time of 60 s. The obtained SAXS profiles were corrected for exposure time, dark current, background scattering, and transmittance. The profiles were displayed as a function of the scattering vector ($q = (4\pi/\lambda)$ sin 2θ, where 2θ is the scattering angle).

2.6. AFM imaging

SPM9700-HT (Shimadzu, Japan) equipped with a silicon cantilever (spring constant: 26 N m^{-1}) was employed. The ion gel was soaked into liquid N_2 and cleaved. At room temperature, the cleaved surface of the sample was observed using AFM in tapping mode to obtain the height and phase images. Fast Fourier transform (FFT) of the resulting AFM phase images was conducted using ImageJ program [24].

3. Results and discussion

3.1. Observation of microstructures

The microphase-separated structures of the ion gels were observed using AFM, as shown in Fig. 2 and Fig. 3. Fig. 2(a) and (b) show the AFM phase images of the 90 wt% SOS-66/[C_2mim][NTf_2] and 60 wt% SOS-84/[C_2mim][NTf_2] ion gels, respectively, (in which structural transition was observed in rheological measurements, *vide infra*) at a cleaved surface after the heating and cooling cycle. In the phase images, the bright and dark areas correspond to soft and hard parts, respectively. That is, the bright area corresponded to the ion-conductive phase composed of PEO and [C_2mim][NTf_2], and the dark area represented the aggregated phase composed of PSt. In both systems, it was found that the ion-conductive phase formed an isotropic network-like continuous phase. The isotropy of the sample was confirmed by the Fourier-transformed image (Fig. S3), which showed an annular pattern and no spots. The domain size (path width) of the ion-conductive phase of the 60 wt% SOS-84/[C_2mim][NTf_2] ion gel was larger than that of the 90 wt % SOS-66/[C_2mim][NTf_2] ion gel, which reflected the volume fraction of the soft segment, φ_{soft} (42.9% and 38.9%, respectively). On the other hand, the aggregated phase also formed a continuous phase without a clear periodic structure and the continuous aggregated phase in 60 wt% SOS-84/[C_2mim][NTf_2] ion gel was clearer than that of 90 wt% SOS-66/[C_2mim][NTf_2] ion gel.

Fig. 4(a) shows the SAXS profile of the 90 wt% SOS-66/[C_2mim][NTf_2] ion gel. A peak appeared at $q = 0.016$ $Å^{-1}$, confirming the presence of a phase-separated structure. Besides, a relationship of $I(q) \sim q^{-4}$ was observed, suggesting that a clear interface was formed between the ion-conducting phase and the aggregated phase. However, higher-order peaks derived from the S, H, and L structures were not observed. From these results, we concluded that a G structure having no clear repeating pattern was formed in this ion gel. Fig. 4(b) shows the SAXS profile of the 60 wt% SOS-84/[C_2mim][NTf_2] ion gel. Here, a higher-order peak corresponding to lamella was observed. On the other hand, in a TEM image (Fig. S4), a network-like structure analogous to the AFM measurement was observed. This result indicates that the lamellar phase coexists with the bicontinuous phase observed by AFM, and therefore, the transition of the elastic modulus is not clear as the pure bicontinuous phase formed in 90 wt% SOS-66/[C_2mim][NTf_2] (see above).

On the other hand, the AFM phase image of the 80 wt% SOS-66/[C_2mim][NTf_2] ion gel (Fig. 3, left), which did not show any unique viscoelastic behavior, showed an H^R structure, in which the ion

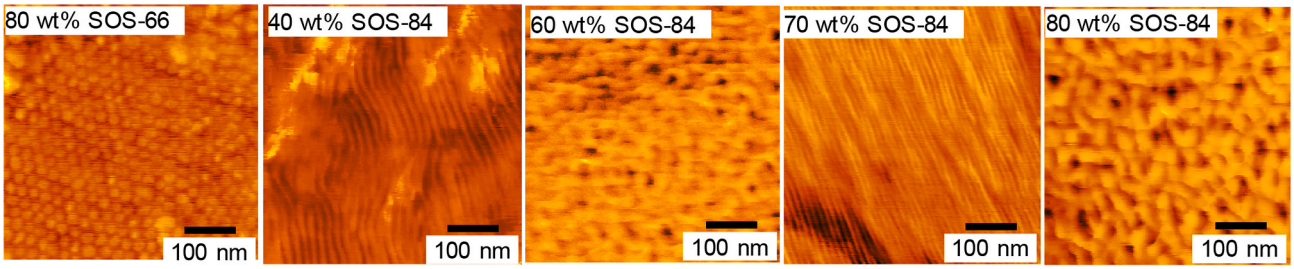

Fig. 3. AFM phase images of SOS-66/[C_2mim][NTf_2] ion gels with various polymer content.

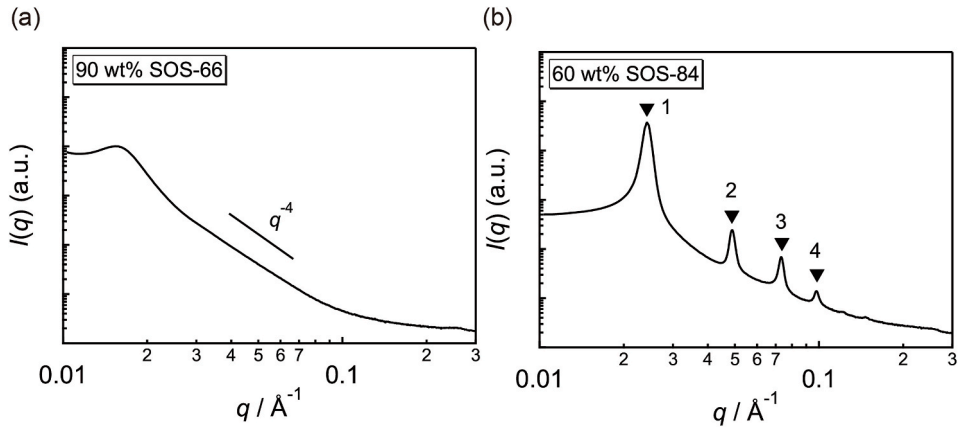

Fig. 4. SAXS profile of (a) 90 wt% SOS-66/[C_2mim][NTf_2] and (b) 60 wt% SOS-84/[C_2mim][NTf_2] ion gels. The periodic peaks can be assigned to lamellar structure (1, 2, 3, 4, …).

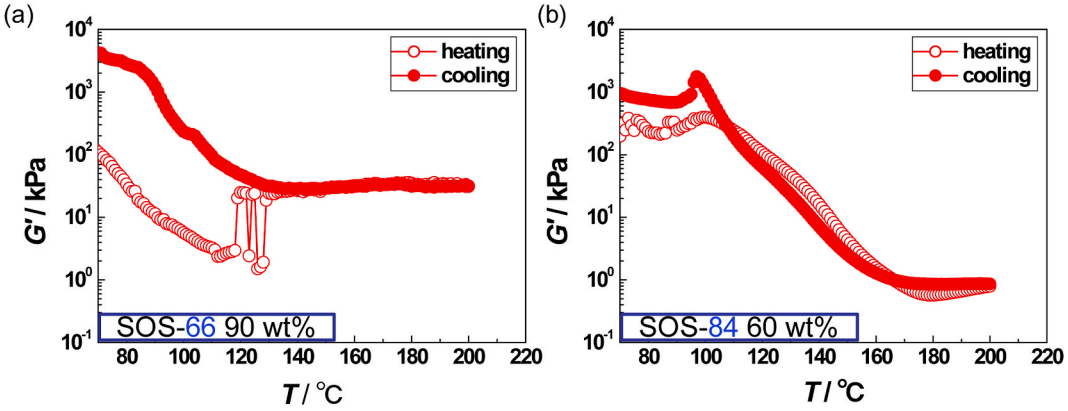

Fig. 5. Temperature sweep measurements of G' for (a) 90 wt% SOS-66/[C_2mim][NTf_2] and (b) 60 wt% SOS-84/[C_2mim][NTf_2] ion gels. Open and close circles correspond to the heating and cooling process, respectively.

conduction phase was cylindrical. In the FFT image of the 80 wt% SOS-66/[C_2mim][NTf_2] ion gel (Fig. S5), hexagonal spots were observed, confirming that it had the H^R structure with a regularity. Various microphase-separated structures, including S, H, L, H^R, and S^R structures were observed by AFM (Fig. 3) and SAXS (Fig. S6). These assignments are listed in Table S1. From the above results, we concluded that G structure could be formed when φ_{soft} is appropriately controlled.

3.2. Transition of the elastic modulus

The results of the temperature sweep rheological measurements for SOS-66 and SOS-84 ion gels with various polymer weight fractions are shown in Fig. 5 and Fig. S7. Fig. 5 shows the profiles for ion gels with G structure, and the profiles exhibited sudden increases in the storage modulus (G') with increasing temperature. Fig. 5(a) shows the temperature dependence of G' of 90 wt% SOS-66/[C_2mim][NTf_2] (the ratio of the soft segment, φ_{soft} = 38.9%). As mentioned in the Introduction, in the diblock copolymer melt system (in the absence of IL, φ_{soft} = 36.5%), a significant increase of G' was observed when a H to G structural transition occurred upon heating [22]. The G' of 90 wt% SOS-66/[C_2mim][NTf_2] decreased with increasing temperature owing to the glass transition of the PSt segments, and then, underwent a sudden increase at 120 °C analogous to the diblock copolymer melt system. The G' was constant at temperatures higher than 120 °C, indicating that the structure was stable even at a high temperature. The high thermal stability of the structure could be ascribed to the high χ value between the PEO with dissolved IL and PSt, which is consistent with previous reports [17]. A large value of the χ parameter indicates the strongly separated hard and soft blocks, which can make ordered microstructures, whereas a small value of the χ parameter indicates that hard and soft blocks easily mix, resulting in a disordered structure. Generally, χ parameter has a temperature dependency, and χ parameter decreases with increasing temperature. Thus, an increase in the temperature often induces the order-disorder transition. However, if the χ parameter is large enough, the microstructure is maintained even at high temperatures, and the order-disorder transition is not observed. In previous papers [17], it is reported that mixing the ionic liquid and the soft segment increases the χ parameter due to the very poor solubility of a polystyrene segment in IL. Thus, the high thermal stability of the microstructure in this study could be ascribed to the analogous effect by the increase of χ parameter.

In the cooling step, G' started increasing at 120 °C, resulting in more than ten times higher G' (4.3 MPa at 70 °C) than that before heating (0.11 MPa at 70 °C). This result indicates that the stable G structure formed continuous glassy PSt segments at a low temperature, which contributed to the high G'.

In the case of the 60 wt% SOS-84/[C_2mim][NTf_2] ion gel (φ_{soft} = 42.9%, Fig. 5(b)), although not as remarkable as SOS-66, an increase of G' with increasing temperature was also observed. This behavior is attributed to the coexistence of different microphase-separated structures (L and G structures), as described later. In the cooling process, a hump was observed at ca. 100 °C. Similar behavior was observed in other ion gels (Fig. S7), and thus, it can be ascribed to the glass transition of PSt block (~100 °C). The transition process seems to be unstable compared with simple diblock copolymer melts because this is a ternary mixture of PEO, PSt, and IL, which can result in bumpy data during glass transition. However, it also showed a high G' of 0.95 MPa at 70 °C, being

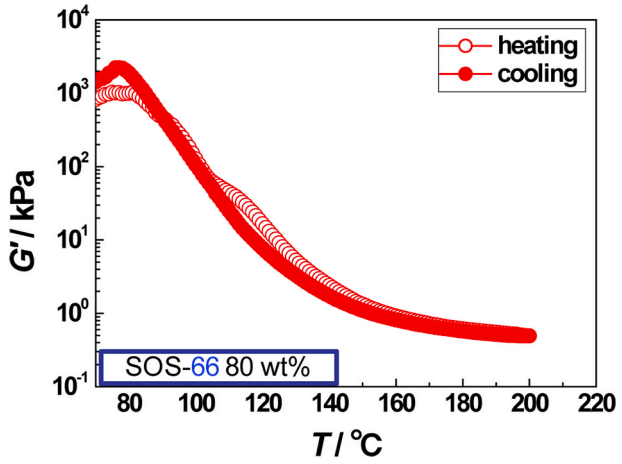

Fig. 6. Temperature sweep measurement of G' for the 80 wt% SOS-66/[C_2mim][NTf_2] ion gel.

five times higher than that before heating. On the other hand, in 80 wt% SOS-66/[C_2mim][NTf_2] (φ_{soft} = 44.1%, Fig. 6) and other ion gels (Fig. S7), G' decreased with increasing temperature, no transition was observed, and the G' values in the heating and cooling processes were almost identical. This result suggests that the H (or L) to G structural transition can also be observed in the ABA-type triblock copolymer-based ion gel system when φ_{soft} is appropriately controlled.

3.3. Dependency of ionic conductivity on the microphase-separated structure

Next, the ionic conductivity of ion gels was measured to evaluate the ion-transport properties of ion gels. Fig. 7 shows the Arrhenius plot of the ionic conductivity (σ) of SOS/[C_2mim][NTf_2] ion gels. For comparison, the ionic conductivity of the PEO solution (σ_0), which contains the same volume fraction of PEO as the corresponding SOS ion gel, is also listed (Table S2). With increasing polymer content, the ionic conductivity decreased. To quantitatively assess the decrease in conductivity, the tortuosity concept was introduced. Tortuosity (τ) is a metric of the complexity of the ion conduction path; the effect of the microphase-separated structure on the ionic conductivity was evaluated in terms of tortuosity. The following equation represents the tortuosity.

$$\tau = \frac{\varphi_{soft}}{\sigma}\sigma_0 \quad (1)$$

where σ is the ionic conductivity of the ion gel, σ_0 is the ionic conductivity of PEO/[C_2mim][NTf_2] solution, τ is the tortuosity factor (randomness of conducting path), and φ_{soft} is the volume fraction of the conducting phase. $\tau = 1$ means that the ionic conduction is not disturbed by the microphase-separated structure of the ion-conductive phase, and the ionic conductivity is equivalent to that of the PEO/IL polymer solution. On the other hand, a large tortuosity implies that the conducting phase is partially disturbed or not connected.

Fig. 8 shows the tortuosity of the ion gels. In general, the connectivity of the ion-conductive path strongly depended on the microphase-separated structures. The S, H, and G structures can form a three-dimensional continuous ion-conductive phase while the L or H^R structures only form two-dimensional or one-dimensional continuous phases, respectively. Furthermore, S^R structures do not have a continuous ion-conductive phase. Indeed, in the case of the S^R structure (80 wt% SOS-84/[C_2mim][NTf_2]), the value was far from 1 (τ = 225), indicating that

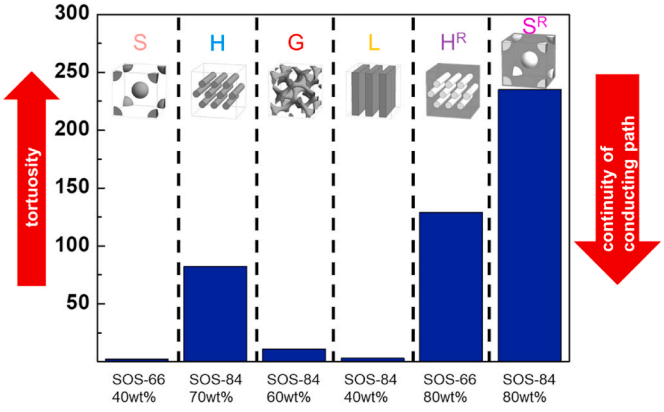

Fig. 8. Tortuosity of the ion gels at each structure. In the schematic illustration, the darker part corresponds to a hard domain.

Table 2
Structure, G', and σ of ion gels with various polymer content.

Polymer/wt%	*Structure*	*G'/kPa* [a]	*σ/mS cm*$^{-1}$ [b]
SOS-66/40 wt%	S	4.68	5.73
SOS-66/80 wt%	H^R	1420	0.014
SOS-66/90 wt%	G	4300	–
SOS-84/40 wt%	L	59	2.51
SOS-84/60 wt%	G + L	950	0.37
SOS-84/70 wt%	H	7660	0.023
SOS-84/80 wt%	S^R	0.141	0.0066

[a] The G' at 70 °C in cooling process.
[b] The σ at 100 °C.

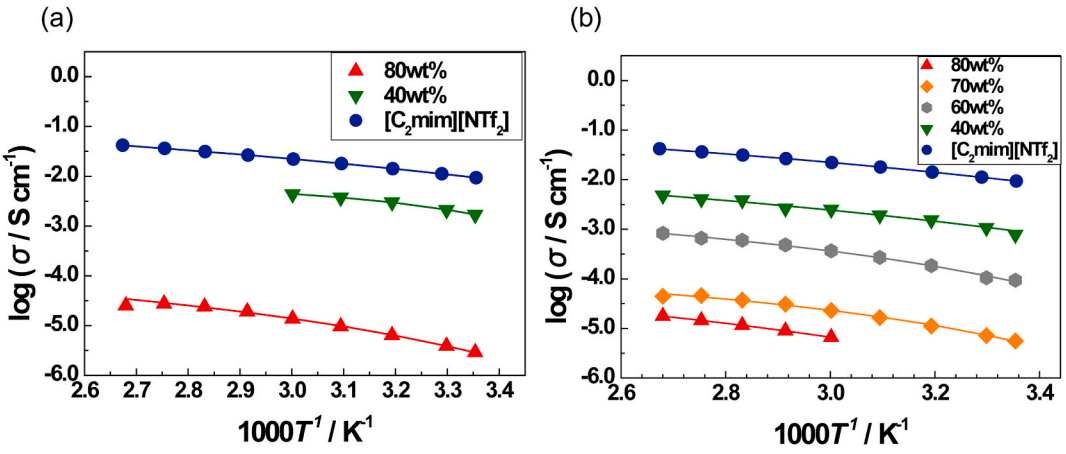

Fig. 7. Ionic conductivity of (a) SOS-66/[C_2mim][NTf_2] and (b) SOS-84/[C_2mim][NTf_2] ion gels.

ion conduction in the S^R structures was negligibly small. Fig. 8 depicts the microphase-separated structures arranged in the inverse order of volume fraction of the ion-conductive phase (left-hand side has higher ion-conductive phase). The structure, mechanical, and transport properties were summarized in Table 2. If the tortuosity is simply determined by the volume fraction, the structures shown on the right-hand side would have higher tortuosity. However, the tortuosity of the S, G, and L structures was exceptionally small. We previously reported that the S structure exhibits low τ value (~1) owing to the high connectivity of the ion-conductive phase as well as three-dimensional isotropic structures [17b]. In H or L structures, the polydomain structure (i.e., randomly packed grains consisting of ordered cylinders or lamellas) disturbed the ion conduction, resulting in a τ value higher than unity. In this study, G and L structures exhibited lower τ values than the H structure, indicating that the conductive phase had few barriers and continued over a long distance. The relatively low τ value of the G structure could be ascribed to the three-dimensionally isotropic ion-conductive phase. However, the tortuosity of the G structure was slightly larger than that of the L structure. As discussed, the G structure in this study also contained the L structure. It is plausible that the increased number of grain boundaries owing to mixed structures increased the tortuosity.

4. Conclusions

We successfully obtained an ion gel that forms a stable bicontinuous structure at room temperature by exploiting the structural transition occurring with increasing temperature. It was found that the ion gel having a bicontinuous structure exhibited favorable mechanical properties ($G' \sim 1.0$ MPa) and good ionic conductivity ($\sigma \sim 0.1$ mS cm^{-1}). Further, its tortuosity was lower than that of the other structures, and showed double minimum values in the S and G, L structures where the conduction phase was less disturbed. Thus, it was concluded that tortuosity depended on the three-dimensional anisotropy of the microphase-separated structures rather than the volume fraction of the ion-conductive phase in such structures. From these results, it was evident that if an ion gel having pure G structure was prepared, the material could be expected to achieve both favorable mechanical properties and ionic conductivity, thus resolving the trade-off problem of polymer electrolyte materials.

Funding

The authors declare no competing financial interest.

CRediT authorship contribution statement

Haruna Mizuno: Writing - original draft. **Kei Hashimoto:** Writing - review & editing. **Kazuhide Ueno:** Formal analysis. **Masayoshi Watanabe:** Supervision, Conceptualization, Writing - review & editing.

Declaration of competing interest

The authors declare that they have no known competing financial interests or personal relationships that could have appeared to influence the work reported in this paper.

Acknowledgments

This work was financially supported by the Grants-in-Aid for Scientific Research S (15H05495) from the Ministry of Education, Culture, Sports, Science and Technology (MEXT) of Japan. The SAXS experiment was performed at the Photon Factory (BL-10C), Tsukuba, Japan (Proposal No. 2017G100 and 2019G055) and SAXS-U, Shibayama Laboratory, Institute for Solid State Physics, The University of Tokyo. TEM observations were conducted at Namiki-Foundry, National Institute for Materials Science in Japan. This work was partially supported by CUPAL frame in NIMS Joint Research Hub Program. We would like to thank Editage (www.editage.com) for English language editing.

Appendix B. Supplementary data

Supplementary data to this article can be found online at https://doi.org/10.1016/j.polymer.2020.122849.

References

[1] a) T. Welton, Room-temperature ionic liquids. Solvents for synthesis and catalysis, Chem. Rev. 99 (1999) 2071–2084;
b) P. Wasserscheid, W. Keim, Ionic liquids—new "solutions" for transition metal catalysis, Angew. Chem., Int. Ed. Engl. 39 (2000) 3772–3789;
c) R.D. Rogers, K.R. Seddon, Ionic liquids-solvents of the future? Science 302 (2003) 792–793;
d) D.R. MacFarlane, N. Tachikawa, M. Forsyth, J.M. Pringle, P.C. Howlett, G. D. Elliott, J.H. Davis, M. Watanabe, P. Simon, C.A. Angell, Energy applications of ionic liquids, Energy Environ. Sci. 7 (2014) 232–250;
e) J.S. Wilkes, A short history of ionic liquids—from molten salts to neoteric solvents, Green Chem. 4 (2002) 73–80;
f) K. Ueno, H. Tokuda, M. Watanabe, Ionicity in ionic liquids: correlation with ionic structure and physicochemical properties, Phys. Chem. Chem. Phys. 12 (2010) 1649–1658.

[2] a) L.A. Blanchard, D. Hancu, E.J. Beckman, J.F. Brennecke, Green processing using ionic liquids and CO_2, Nature 399 (1999) 28–29;
b) M. Ramdin, T.W. de Loos, T.J.H. Vlugt, State-of-the-Art of CO_2 capture with ionic liquids, Ind. Eng. Chem. Res. 51 (2012) 8149–8177;
c) J.E. Bara, D.E. Camper, D.L. Gin, R.D. Noble, Room-temperature ionic liquids and composite materials: platform technologies for CO2 capture, Acc. Chem. Res. 43 (2010) 152–159;
d) J.E. Bara, T.K. Carlisle, C.J. Gabriel, D. Camper, A. Finotello, D.L. Gin, R. D. Noble, Guide to CO_2 separations in imidazolium-based room-temperature ionic liquids, Ind. Eng. Chem. Res. 48 (2009) 2739–2751;
e) M. Hasib-ur-Rahman, M. Siaj, F. Larachi, Ionic liquids for CO_2 capture—development and progress, Chem. Eng. Process 49 (2010) 313–322.

[3] a) K.D. Clark, M.J. Trujillo-Rodriguez, J.L. Anderson, Advances in the analysis of biological samples using ionic liquids, Anal. Bioanal. Chem. 410 (2018) 4567–4573;
b) C.J. Clarke, W.C. Tu, O. Levers, A. Brohl, J.P. Hallett, Green and sustainable solvents in chemical processes, Chem. Rev. 118 (2018) 747–800;
c) H. Wang, G. Gurau, R.D. Rogers, Ionic liquid processing of cellulose, Chem. Soc. Rev. 41 (2012) 1519–1537;
d) A. Kumar, P. Venkatesu, Innovative aspects of protein stability in ionic liquid mixtures, Biophys. Rev. 10 (2018) 841–846;
e) H. Passos, M.G. Freire, J.A. Coutinho, Ionic liquid solutions as extractive solvents for value-added compounds from biomass, Green Chem. 16 (2014) 4786–4815.

[4] a) J. Lu, F. Yan, J. Texter, Advanced applications of ionic liquids in polymer science, Prog. Polym. Sci. 34 (2009) 431–448;
b) T. Ueki, M. Watanabe, Polymers in ionic liquids: dawn of neoteric solvents and innovative materials, Bull. Chem. Soc. Jpn. 85 (2012) 33–50.

[5] a) C.S. Brazel, R.D. Rogers, Ionic Liquids in Polymer Systems: Solvents, Additives, and Novel Applications, American Chemical Society, Washington, DC, 2005;
b) N. Winterton, Solubilization of polymers by ionic liquids, J. Mater. Chem. 16 (2006) 4281–4293.

[6] a) W. Lu, A.G. Fadeev, B. Qi, E. Smela, B.R. Mattes, J. Ding, G.M. Spinks, J. Mazurkiewicz, D. Zhou, G.G. Wallace, D.R. MacFarlane, S.A. Forsyth, M. Forsyth, Use of ionic liquids for pi-conjugated polymer electrochemical devices, Science 297 (2002) 983–987;
b) M.D. Bennett, D.J. Leo, Ionic liquids as stable solvents for ionic polymer transducers, Sen. Actuators A Phys. 115 (2004) 79–90;
c) B.J. Akle, M.D. Bennett, D.J. Leo, High-strain ionomeric–ionic liquid electroactive actuators, Sen. Actuators A Phys. 126 (2006) 173–181;
d) D. Zhou, G.M. Spinks, G.G. Wallace, C. Tiyapiboonchaiya, D.R. MacFarlane, M. Forsyth, J. Sun, Solid state actuators based on polypyrrole and polymer-in-ionic liquid electrolytes, *Electrochim*, Acta 48 (2003) 2355–2359;
e) T. Fukushima, K. Asaka, A. Kosaka, T. Aida, Fully plastic actuator through layer-by-layer casting with ionic-liquid-based bucky gel, Angew. Chem., Int. Ed. Engl. 44 (2005) 2410–2413;
f) K. Mukai, K. Asaka, K. Kiyohara, T. Sugino, I. Takeuchi, T. Fukushima, T. Aida, High performance fully plastic actuator based on ionic-liquid-based bucky gel, Electrochim. Acta 53 (2008) 5555–5562.

[7] J.E. Bara, E.S. Hatakeyama, C.J. Gabriel, X. Zeng, S. Lessmann, D.L. Gin, R. D. Noble, Synthesis and light gas separations in cross-linked gemini room temperature ionic liquid polymer membranes, J. Membr. Sci. 316 (2008) 186–191.

[8] a) A. Lewandowski, Electrochemical capacitors with polymer electrolytes based on ionic liquids, Solid State Ionics 161 (2003) 243–249;
b) Y. Isshiki, M. Nakamura, S. Tabata, K. Dokko, M. Watanabe, Electric double-layer capacitance of inverse opal carbon prepared through carbonization of poly (furfuryl alcohol) in contact with polymer gel electrolyte containing ionic liquid, *polym*, Adv. Met. Technol. 22 (2011) 1254–1260.

[9] a) H. Shobukawa, H. Tokuda, M.A.H. Susan, M. Watanabe, Ion transport properties of lithium ionic liquids and their ion gels, Electrochim. Acta 50 (2005) 3872–3877;
b) J.-H. Shin, W.A. Henderson, S. Passerini, PEO-based polymer electrolytes with ionic liquids and their use in lithium metal-polymer electrolyte batteries, J. Electrochem. Soc. 152 (2005) A978;
c) H. Ye, J. Huang, J.J. Xu, A. Khalfan, S.G. Greenbaum, Li ion conducting polymer gel electrolytes based on ionic liquid/PVDF-HFP blends, J. Electrochem. Soc. 154 (2007) A1048.

[10] a) S.Y. Lee, T. Yasuda, M. Watanabe, Fabrication of protic ionic liquid/sulfonated polyimide composite membranes for non-humidified fuel cells, J. Power Sources 195 (2010) 5909–5914;
b) S.Y. Lee, A. Ogawa, M. Kanno, H. Nakamoto, T. Yasuda, M. Watanabe, Nonhumidified intermediate temperature fuel cells using protic ionic liquids, J. Am. Chem. Soc. 132 (2010) 9764–9773.

[11] a) P. Wang, S.M. Zakeeruddin, I. Exnar, M. Gratzel, High efficiency dye-sensitized nanocrystalline solar cells based on ionic liquid polymer gel electrolyte, Chem. Commun. (2002) 2972–2973;
b) R. Kawano, T. Katakabe, H. Shimosawa, M. Khaja Nazeeruddin, M. Grätzel, H. Matsui, T. Kitamura, N. Tanabe, M. Watanabe, Solid-state dye-sensitized solar cells using polymerized ionic liquid electrolyte with platinum-free counter electrode, Phys. Chem. Chem. Phys. 12 (2010) 1916–1921.

[12] a) T.H. Kang, H. Chae, Y. Ahn, D. Kim, M. Lee, G.R. Yi, Free-standing ion-conductive gels based on polymerizable imidazolium ionic liquids, Langmuir 35 (2019) 16624–16629;
b) L.D. McIntosh, M.W. Schulze, M.T. Irwin, M.A. Hillmyer, T.P. Lodge, Evolution of morphology, modulus, and conductivity in polymer electrolytes prepared via polymerization-induced phase separation, Macromolecules 48 (2015) 1418–1428;
c) S.A. Chopade, S. So, M.A. Hillmyer, T.P. Lodge, Anhydrous proton conducting polymer electrolyte membranes via polymerization-induced microphase separation, ACS Appl. Mater. Interfaces 8 (2016) 6200–6210.

[13] a) K. Fujii, H. Asai, T. Ueki, T. Sakai, S. Imaizumi, U. Chung, M. Watanabe, M. Shibayama, High-performance ion gel with tetra-PEG network, Soft Matter 8 (2012) 1756–1759;
b) K. Hashimoto, K. Fujii, K. Nishi, T. Sakai, M. Shibayama, Nearly ideal polymer network ion gel prepared in pH-buffering ionic liquid, Macromolecules 49 (2016) 344–352;
c) S. Ishii, H. Kokubo, K. Hashimoto, S. Imaizumi, M. Watanabe, Tetra-PEG network containing ionic liquid synthesized via michael addition reaction and its application to polymer actuator, Macromolecules 50 (2017) 2906–2915.

[14] a) F. Ranjbaran, E. Kamio, H. Matsuyama, Ion gel membrane with tunable inorganic/organic composite network for CO_2 separation, Ind. Eng. Chem. Res. 56 (2017) 12763–12772;
b) X. Liu, B. He, Z. Wang, H. Tang, T. Su, Q. Wang, Tough nanocomposite ionogel-based actuator exhibits robust performance, Sci. Rep. 4 (2014) 6673.

[15] a) F. Moghadam, E. Kamio, A. Yoshizumi, H. Matsuyama, An amino acid ionic liquid-based tough ion gel membrane for CO_2 capture, Chem. Commun. 51 (2015) 13658–136561;
b) Z. Tang, X. Lyu, A. Xiao, Z. Shen, X. Fan, High-Performance double-network ion gels with fast thermal healing capability via dynamic covalent bonds, Chem. Mater. 30 (2018) 7752–7759;
c) L. Yu, S. Guo, Y. Lu, Y. Li, X. Lan, D. Wu, R. Li, S. Wu, X. Hu, Highly tough, Li-metal compatible organic–inorganic double-network solvate ionogel, Adv. Energy Mater. 9 (2019), 1900257.

[16] a) S. Imaizumi, H. Kokubo, M. Watanabe, Polymer actuators using ion-gel electrolytes prepared by self-assembly of ABA-triblock copolymers, Macromolecules 45 (2012) 401–409;
b) R. Tamate, K. Hashimoto, T. Ueki, M. Watanabe, Block copolymer self-assembly in ionic liquids, Phys. Chem. Chem. Phys. 20 (2018) 25123–25139.

[17] a) T.M. Bennett, K.S. Jack, K.J. Thurecht, I. Blakey, Perturbation of the experimental phase diagram of a diblock copolymer by blending with an ionic liquid, Macromolecules 49 (2015) 205–214;
b) K. Hashimoto, M. Hirasawa, H. Kokubo, R. Tamate, X. Li, M. Shibayama, M. Watanabe, Transport and mechanical properties of ABA-type triblock copolymer ion gels correlated with their microstructures, Macromolecules 52 (2019) 8430–8439.

[18] a) J.H. Choi, Y.S. Ye, Y.A. Elabd, K.I. Winey, Network structure and strong microphase separation for high ion conductivity in polymerized ionic liquid block copolymers, Macromolecules 46 (2013) 5290–5300;
b) P.M. Simone, T.P. Lodge, Phase behavior and ionic conductivity of concentrated solutions of polystyrene-poly(ethylene oxide) diblock copolymers in an ionic liquid, ACS Appl. Mater. Interfaces 1 (2009) 2812–2820;
c) L. Gwee, J.H. Choi, K.I. Winey, Y.A. Elabd, Block copolymer/ionic liquid films: the effect of ionic liquid composition on morphology and ion conduction, Polymer 51 (2010) 5516–5524;
d) K.-H. Shen, J.R. Brown, L.M. Hall, Diffusion in lamellae, cylinders, and double gyroid block copolymer nanostructures, ACS Macro Lett. 7 (2018) 1092–1098;
e) R.L. Weber, Y.S. Ye, A.L. Schmitt, S.M. Banik, Y.A. Elabd, M.K. Mahanthappa, Effect of nanoscale morphology on the conductivity of polymerized ionic liquid block copolymers, Macromolecules 44 (2011) 5727–5735;
f) M.T. Irwin, R.J. Hickey, S. Xie, S. So, F.S. Bates, T.P. Lodge, Structure–conductivity relationships in ordered and disordered salt-doped diblock copolymer/homopolymer blends, Macromolecules 49 (2016) 6928–6939.

[19] a) S.C. Price, X. Ren, A.C. Jackson, Y. Ye, Y.A. Elabd, F.L. Beyer, Bicontinuous alkaline fuel cell membranes from strongly self-segregating block copolymers, Macromolecules 46 (2013) 7332–7340;
b) M.T. Irwin, R.J. Hickey, S. Xie, F.S. Bates, T.P. Lodge, Lithium salt-induced microstructure and ordering in diblock copolymer/homopolymer blends, Macromolecules 49 (2016) 4839–4849;
c) S. Xie, D.J. Meyer, E. Wang, F.S. Bates, T.P. Lodge, Structure and properties of bicontinuous microemulsions from salt-doped ternary polymer blends, Macromolecules 52 (2019) 9693–9702.

[20] a) C.-Y. Wang, T.P. Lodge, Kinetics and mechanisms for the cylinder-to-gyroid transition in a block copolymer solution, Macromolecules 35 (2002) 6997–7006;
b) M.E. Vigild, K. Almdal, K. Mortensen, I.W. Hamley, J.P.A. Fairclough, A. J. Ryan, Transformations to and from the gyroid phase in a diblock copolymer, Macromolecules 31 (1998) 5702–5716;
c) K.J. Hanley, T.P. Lodge, Effect of dilution on a block copolymer in the complex phase window, J. Polym. Sci. B 36 (1998) 3101–3113;
d) S.C. Schmidt, M.A. Hillmyer, Morphological behavior of model poly(ethylene-alt-propylene)-b-polylactide diblock copolymers, J. Polym. Sci. B 40 (2002) 2364–2376;
e) I.W. Hamley, J.P.A. Fairclough, A.J. Ryan, S.M. Mai, C. Booth, Lamellar-to-gyroid transition in a poly(oxyethylene)–poly(oxybutylene) diblock copolymer melt, Phys. Chem. Chem. Phys. 1 (1999) 2097–2101;
f) D.A. Hajduk, H. Takenouchi, M.A. Hillmyer, F.S. Bates, M.E. Vigild, K. Almdal, Stability of the perforated layer (PL) phase in diblock copolymer melts, Macromolecules 30 (1997) 3788–3795.

[21] M.B. Kossuth, D.C. Morse, F.S. Bates, Viscoelastic behavior of cubic phases in block copolymer melts, J. Rheol. 43 (1999) 167–196.

[22] H. Mao, M.A. Hillmyer, Macroscopic samples of polystyrene with ordered three-dimensional nanochannels, Soft Matter 2 (2006) 57–59.

[23] A. Noda, K. Hayamizu, M. Watanabe, Pulsed-gradient spin-echo H-1 and F-19 NMR ionic diffusion coefficient, viscosity, and ionic conductivity of non-chloroaluminate room-temperature ionic liquids, J. Phys. Chem. B 105 (2001) 4603–4610.

[24] C.A. Schneider, W.S. Rasband, K.W. Eliceiri, NIH Image to ImageJ: 25 years of image analysis, Nat. Methods 9 (2012) 671–675.